Published in *Coastal Engineering Journal*, 2021/10/2

Evaluating XBeach performance for extreme offshore-directed sediment transport events on a dissipative beach

Takayuki Suzuki [a*] and Daniel T. Cox [b]
a* Department of Civil Eng., Yokohama National University, Yokohama, Japan, suzuki-t@ynu.ac.jp
b School of Civil and Construction Eng., Oregon State University, Corvallis, USA Dan.Cox@oregonstate.edu

Abstract

The performance of the process-based nearshore model XBeach for predicting extreme offshore-directed sediment transport was investigated using field observations at a dissipative beach in Japan. Three extreme erosion events were identified from a record of 6,209 observations of the cross-shore profile change at Hasaki, Japan, from 1987 to 2003. The analysis considered the sensitivity of the wave nonlinearity of short waves that could be tuned using the parameter, f_{ua}, to the observed bed profile change. The comparisons revealed that for extreme offshore-directed sediment transport events, f_{ua} = 0.0 is the best fit for predicting these extreme beach profile changes. In the nearshore zone, erosion was underestimated, and the BSS exhibited low values. Peak sediment deposition occurred in the bar-offshore zone with sediments transported from the nearshore zone and was estimated by the model reasonably well. In addition to the three extreme events, 14 other large events were identified, and the trends of beach profile change could be estimated with sufficient tuning of the f_{ua} parameter. After analyzing the correlation between f_{ua} and wave and morphology-related parameters, the f_{ua} value could be correlated to the observed volume change. This suggested that if there were a rough estimate of the expected total volume change, this may help in setting f_{ua} value.

Keywords: cross-shore sediment transport, beach profile change, volume change, field data

1. Introduction

Sediments are dynamically transported in onshore and offshore directions in coastal areas, especially in the foreshore and nearshore zones. Managing both types of sediment transport is important for coastal problems, such as beach erosion and accretion. Moreover, the foreshore and nearshore zones are the regimes where the public interacts with the ocean during recreational and leisure activities. Therefore, estimating the beach profile change of these zones is of paramount importance for disaster prevention of natural catastrophic events, such as storms and storm surges, as well as for recreation and habitat.

Sediment transport rates in the foreshore zone (e.g., Baldock et al., 2011; Puleo et al., 2000; Suzuki et al., 2007) and nearshore zones (e.g., Deigaard et al., 1986; Elgar et al., 2001) have been investigated, and numerical models for these zones have been proposed (e.g., Bailard, 1981; Jayaratne et al., 2014; Kelly and Dodd, 2010; Larson et al., 2004). Several process-based beach profile evolution models have been proposed, including SBeach (Larson and Kraus, 1989), CShore (Kobayashi and Farhadzadeh, 2008; Figlus et al., 2011), and XBeach (Roelvink et al., 2009). While there is no universally accepted model, this study focuses on XBeach because it is more widely used globally than SBeach and CShore in recent years and because the source code is easily available. The model includes the hydrodynamic processes of short wave and long wave transformations, wave-induced setup, and unsteady currents, overwash and inundation, and the morphodynamic processes, including the effects of vegetation and hard structures.

The XBeach model predicts the coastal morphological response due to the time-varying wave and water level conditions. XBeach is under continuous development as an open-source model, including numerical schemes for swash zone dynamics (Roelvink et al., 2018), dune erosion events, and overwash. Table 1 summarizes some of the recent XBeach research and information about geographic location, morphological time scale, sediment diameter, a targeted region in the coastal zone, and hydrodynamic parameters.

The evolution time scales in these studies vary from a few hours (e.g., Elsayed and Oumeraci, 2017) to several years (e.g., Faraci et al., 2014). XBeach has been shown to have good applicability for both short and medium timescales of morphology change. XBeach has been frequently applied to the field observations (e.g., de Vet et al., 2015), large-scale laboratory experiments (e.g., Do et al., 2018), and smaller-scale experiments (e.g., Berard et al., 2017), and most of the cases were applied to dune erosion.

XBeach was originally developed to simulate the impact of storms and hurricanes on sandy beaches, with an emphasis on foreshore profile change, dune erosion, and overwash. For dune erosion, the model has been applied to several different coasts and shows reasonable results of beach profile change with some tuning of parameters (e.g., Splinter and Palmsten, 2012; Armaroli et al., 2013; de Winter et al., 2015). For overwash events, XBeach has been shown to predict both erosion and accretion of the foreshore profile (e.g., McCall et al., 2010; Williams et al., 2015) with necessary parameter tuning. XBeach has been applied to the swash and inner-bar zone of sediment movement under erosive conditions (e.g., Bolle et al., 2011; Vousdoukas et al., 2011; Dissanayake et al., 2014). Comparison with observations showed that the predicted profile changes were less accurate than the dune erosion cases. There have been relatively few cases of accretion. Pender and Karunarathna (2013) reported that XBeach predicted post-storm recovery reasonably well.

For the cross-shore sediment transport, it is suggested that the effect of wave nonlinearity is important (e.g., Bugajny et al., 2013; Nederhoff et al., 2015). In XBeach, wave nonlinearity parameter f_{ua} plays an important role for cross-shore sediment transport. Elsayed and Oumeraci (2017) suggested using the average beach slope steepness to determine the parameter f_{ua} for dune erosion. Rafati et al. (2021) adjusted the f_{ua} and other coefficients, and improved the agreement of the computed results with observed wave heights, offshore-directed mean currents (undertow), the wave-orbital-velocity third moments (skewness and asymmetry), and onshore/offshore sandbar migration.

In summary, XBeach has been extensively used for cross-shore sediment transport over a range of time scales and morphologies. However, a fair amount of tuning is required (e.g., Palmsten and Splinter, 2016), and the universal nature of these coefficients is uncertain for both onshore and offshore-directed transport conditions. This study focuses on this aspect by carefully selecting field data for which there is only offshore-directed transport and investigating the sensitivity of short wave nonlinearity parameter, f_{ua}, on beach profile change using extreme offshore-directed sediment transport events. Moreover, we attempt to determine a predictive relationship for f_{ua} based on incident wave conditions, grain size, and total volume of sediment transport.

Table 1. Summary of XBeach application for beach profile change using field and large-scale experimental data.

ID	authors	year	Lab/Field	location		duration	d_{50} [mm]	Event/transport direction	Version	dune	berm, inner-bar	outer-bar	profile	WL, aveH	Hs	velocity	volume, resession	runup	ground-water
a1	Roelvink et al.	2009	Lab	Netherlands	Delta flume	6, 8 h	0.2	Dune erosion	1D, 2D	x	x		x	x	x	x	x		
a2			Field	USA	Maryland	20 h	n/a	Overwash		x	x		x						
b	Lindemer et al.	2010	Field	USA	Barrir Is.	60.5 h	n/a	Overwash	2D	x	x		x						
c	McCall et al.	2010	Field	USA	Santa Rosa	36 h	0.2	Overwash	2D	x	x		x				x		
d	de Alegria-Arzaburu et a	2010	Field	UK	Slapton Sands	68 h	6	Dune erosion, Overwash	1D	x	x		x						
e	Bolle et al.	2011	Field	Belgium	Ostend	50 h	n/a	Erosion	1D, 2D		x		x						
f	Vousdoukas et al.	2011	Field	Poltugal	Faro Beach	12-18 h	0.5	Erosion	1D	x	x		x						
g	Splinter and Palmsten	2012	Field	Australia	Gold Coast	160 h	0.25	Dune erosion	2D	x			x				x		
h1	Williams et al.	2012	Lab	Netherlands	Delta Flume BARDEX	3-6 h	11	Dune erosion, Overwash	1D	x	x		x	x			x		x
h2			Field	UK	Slapton Sands	70 h	6	Dune erosion, Overwash	1D	x	x		x	x			x		x
i	Armaroli et al.	2013	Field	Italy	Emilia-Romagna	26-41 h	0.21	Dune erosion	2DH	x	x		x						
j	Callaghan et al.	2013	Field	Australia	Collaroy/Narrabeen	29-72 d	0.35	Erosion			x		x				x		
k1	Pender and Karunarathn	2013	Field	Australia	Narrabeen	49.5 h	0.37	Erosion	2D		x		x				x		
k2			Field	Australia	Narrabeen	24.5 d	0.37	Accretion	2D		x		x				x		
l	Dissanayake et al.	2014	Field	UK	Sefton Coast	8 d	0.2	Erosion	1D, 2D	x	x		x				x		
m	Faraci et al.	2014	Field	Italy	Belvedere Marittimo	2 y	3	Erosion	1D		x		x						
n1	Jamal et al.	2014	Lab	Germany	GWK	2.7 h	21	Berm formation	V12, 1DH		x		x			x			
n2			Field	UK	Christchurch	22 h	7.2	Berm formation	V12, 1DH		x		x						
o	Splinter et al.	2014	Field	Australia	Gold Coast	24.75 d	n/a	Dune erosion	V18	x			x				x		
p	Verheyen et al.	2014	Field	Ghana	Ada	1 y	0.54	Dune erosion	1DH	x	x		x						
q	de Vet et al.	2015	Field	USA	New York	48 h	0.4	Dune erosion, Overwash	2DH	x			x						
r	de Winter et al.	2015	Field	Netherlands	Egmond	75 h	0.3	Dune erosion	2D, V19	x			x				x		
s	Williams et al.	2015	Field	Ireland	Rossbeigh	24 h	0.235	Overwash	1D, 2D	x			x				x		
t	Palmsten and Splinter	2016	Lab	USA	OSU	16 h	0.23	Dune erosion	1D, V18	x			x	x	x			x	
u	de Winter and Ruessink	2017	Field	Netherlands	Egmond, Noorwijk	5 h	0.2	Dune erosion	2D, V19	x			x	x		x	x		
v1	Elsayed and Oumeraci	2017	Lab	Germany	GWK	1.59 h	0.16	Dune erosion	2D	x			x				x		
v2			Field	USA	Santa Rosa	36 h	0.2	Overwash	2D	x			x				x		
w	Do et al.	2018	Lab	USA	OSU	2.15 h	0.2	Dune erosion	1D	x	x		x				x		
x	Schambach et al.	2018	Field	USA	Rhode Island	45 h	0.58	Dune erosion	2D	x			x				x		
y	Yin et al.	2019	Field	China	Xiamen Island	26 h	0.386	Offshore	1 D		x		x	x					
z	Schweiger et al.	2020	Field	Germany	Rostck-Warnemude	30 h	0.3	Onshore, offshore	2DH	x	x		x	x	x		x		
aa	Rafati et al.	2021	Field	USA	near Duck	4-5 d	0.2	Onshore, offshore	1D		x	x	x	x		x			
A	**Present research**		Field	Japan	Hasaki Coast	3 d	0.18	Onshore, offshore	1D, Kings		x	x	x	x	x				

2. XBeach Model

In the present study, we used the Kingsday version of the XBeach model in hydrostatic mode. Details of the model can be found in the online documentation of XBeach, and this section briefly explains the sediment transport equations, which are the subject of this investigation.

The shallow water momentum equation (wave action balance) is given by:

$$\frac{\partial A}{\partial t}+\frac{\partial c_x A}{\partial x}+\frac{\partial c_y A}{\partial y}+\frac{\partial c_\theta A}{\partial t}=-\frac{D_w+D_f}{\sigma} \tag{1}$$

where x is the cross-shore direction, y is the alongshore direction, c_x and c_y are the wave propagation speeds in the x and y directions, respectively, A is the parameter of wave action, which is the ratio between the wave energy density and intrinsic wave frequency, D_w and D_f are dissipation terms for the waves and bottom friction, σ is the intrinsic wave frequency, θ is the wave angle with respect to the x-axis, and t is time.

Three different wave-breaking formulations for nonstationary wave conditions have been implemented in XBeach and affect the wave dissipation term, D_w, the original formulation of Roelvink (1993), an extended version described in Roelvink (1993), and a formulation following Daly et al. (2010). The wave dissipation term of Roelvink-extended (default) is given as

In this study, based on previous investigations (Suzuki and Cox, 2019), the formulation of Daly et al. was used for the analysis. The wave breaking formation of Daly et al. is given as

$$D_w=2\frac{\alpha}{T_{rep}}Q_b E_w \frac{H_{rms}}{h} \tag{2}$$

$$Q_b=1-\exp\left(-\left(H_{rms}/H_{\max}\right)^n\right) \tag{3}$$

$$H_{\max}=\gamma(h+\delta H_{rms}) \tag{4}$$

where α is the wave dissipation coefficient, T_{rep} is the representative wave period, Q_b is the fraction of wave breaking, ρ is the water density, and E_w is the energy density of the wave. The maximum wave height is calculated as a ratio of the water depth plus a fraction of the wave height (δH_{rms}) using a breaker index γ. Alternatively, the formulation of Daly et al. states that waves are fully breaking if the wave height exceeds a threshold (γ) and stop breaking if the wave height falls below another threshold (γ_2). The fraction of wave breaking, Q_b, is determined by:

$$Q_b = \begin{cases} 1 & if \quad H_{rms} > \gamma h \\ 0 & if \quad H_{rms} < \gamma_2 h \end{cases} \tag{5}$$

The default values of the parameters γ and γ_2 were 0.55 and 0.10, respectively.

Sediment concentrations in the water column are modeled using a depth-averaged advection-diffusion scheme with a source-sink term based on equilibrium sediment concentrations (Galappatti and Vreugdenhil, 1985), and the effect of wave skewness and asymmetry are accounted for in the advection-diffusion equation given by

$$\frac{\partial hC}{\partial t} + \frac{\partial hC(u^E - u_a \sin\theta)}{\partial x} + \frac{\partial hC(v^E - u_a \cos\theta)}{\partial y} + \frac{\partial}{\partial x}\left[D_h h \frac{\partial C}{\partial x}\right] + \frac{\partial}{\partial y}\left[D_h h \frac{\partial C}{\partial y}\right] = -\frac{hC_{eq} - hC}{T_a} \tag{6}$$

where C is the depth-averaged sediment concentration, C_{eq} is the total equilibrium sediment concentration, u^E and v^E are the Eulerian cross-shore and longshore velocities, respectively, D_h is the sediment diffusion coefficient, θ is the wave angle, and T_a is the adaptation time. XBeach does not simulate the wave shape of short (gravity) waves; hence, the sediment advection velocity, u_a, is included to account for wave shape effects on sediment transport and is given as

$$u_a = (f_{Sk} S_k - f_{As} A_s) u_{rms} \tag{7}$$

The advection velocity u_a is calculated as a function of wave skewness (S_k), wave asymmetry (A_s), root-mean-square velocity u_{rms}, and two calibration factors f_{Sk} and f_{As}. A higher value of u_a will simulate a stronger onshore sediment transport component. Both f_{Sk} and f_{As} can be set to the same value using the parameter f_{ua}, i.e., $f_{ua} = f_{Sk} = f_{As}$, and a lot of researchers calibrate using f_{ua}. In summary, XBeach contains several tuning parameters, including f_{ua} and f_{mor}. This study focuses on f_{ua} and whether it can be held constant for extreme offshore-directed erosion events.

3. Methodology

3.1 Field Observations

The study site is a natural sandy beach on the Hasaki coast of Japan, facing the Pacific Ocean and angled 31 degrees anti-clockwise from the north, as depicted in Figure 1. In this research, *x* positive is set as the seaward distance perpendicular to the shore, and *y* positive is set as 90 degrees clockwise direction, parallel to the shore (Fig. 1). The *x*-*y* origin was set near the shoreline. The study site includes the Hazaki Oceanographical Research Station (HORS), which maintains a 427 m long research pier positioned perpendicular to the shore. The pier was constructed in 1986 and has been in continuous operation for nearshore processes research, including measurements of nearshore hydrodynamics and morphological responses (e.g., Kuriyama, 2002; Suzuki et al., 2009).

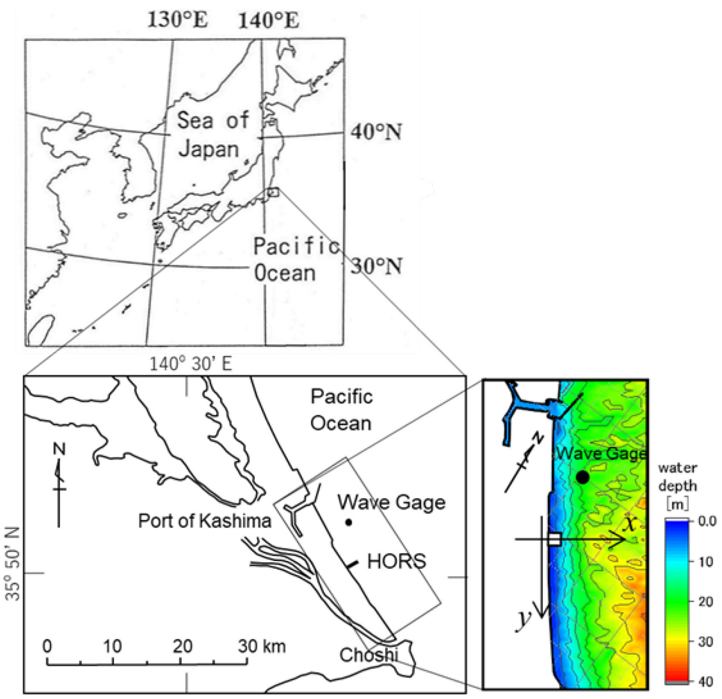

Figure 1. Location of study site of Hazaki Oceanographical Research Station (HORS) on the Hasaki coast of Japan facing the Pacific Ocean, and detailed bathymetry (Japan Oceanographic Data Center) around the HORS.

Beach profiles along the pier were measured at 5 m intervals from March 1986 to the present, following the procedure established by Katoh and Yanagishima (1988) using a 3 kg lead weight from above the pier and using a level and staff landward of the pier. Surveys were conducted every weekday from March 1986 to March 2011, and once a week thereafter. The longshore currents along the pier were measured together with a beach profile survey using a spherical float with a diameter of 0.2 m, 1 m below the water surface. Kuriyama et al. (2008) confirmed the accuracy of the current measurements by comparing the float measurements with data from an electromagnetic current meter, and the correlation coefficient R was 0.97. The median sediment diameter of the coast was 0.18 mm, and it was almost uniform along the pier (Katoh and Yanagishima, 1995).

Wave data were observed at three locations on the pier (x = 40 m, 145 m, and 380 m) using an ultrasonic gage and at one location offshore of the Port of Kashima (dot in Fig. 1) using an ultrasonic sensor. The offshore wave gage was located approximately 8 km north of the HORS pier at a water depth of 24 m to provide continuous observations of the wave height, period, and direction in deeper water. The significant wave height and significant wave period were calculated hourly using a 20-min sample (Suzuki et al., 2019). The wave direction was observed only at the offshore location. Therefore, the wave direction at the end of the pier was estimated using Snell's law, and the wave condition offshore of the Port of Kashima was assumed to represent the wave conditions offshore of the pier based on previous numerical modeling work by Kuriyama (2012).

The water level data were recorded hourly at the end of the pier. The high, mean, and low water levels based on the datum level (D.L.) at the Hasaki coast (Tokyo Peil - 0.687 m) were 1.25, 0.65, and -0.20 m, respectively. Figure 2 presents an example of the wave, current, and water level of October 12–22, 1990, corresponding to one of the comparison cases discussed later.

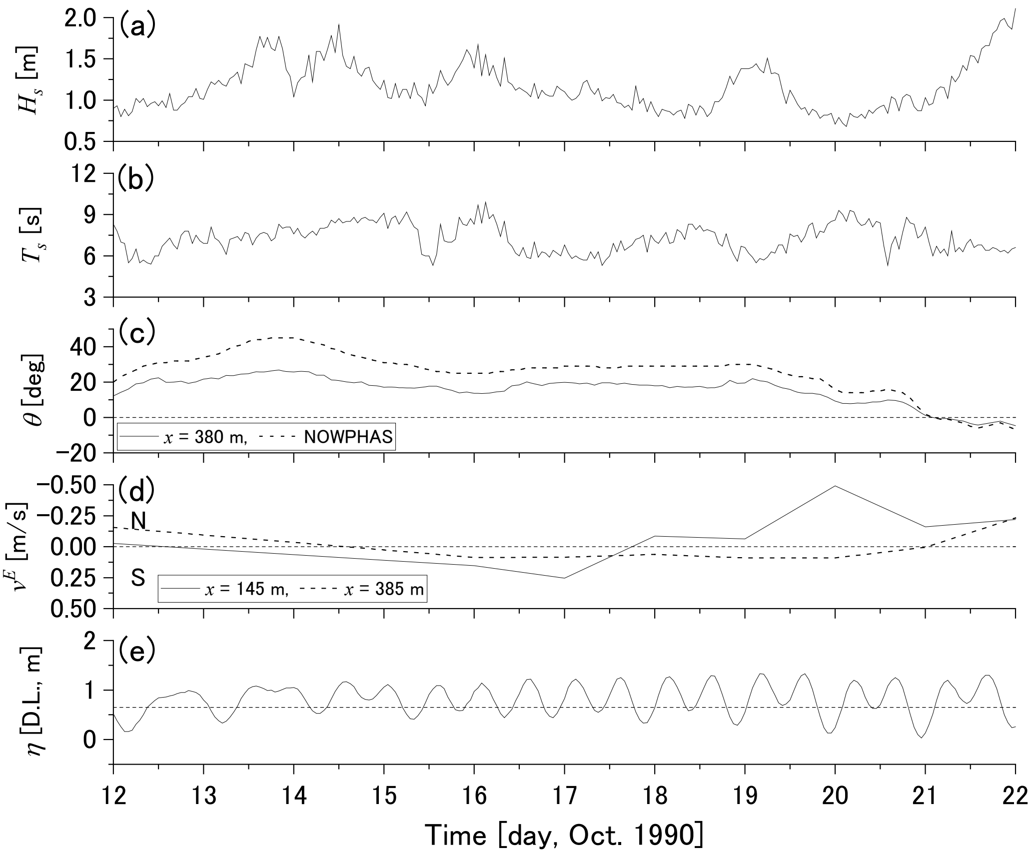

Figure 2: Observed data from Oct. 12-22, 1990. (a) wave height, (b) wave period, (c) wave direction, (d) longshore current, and (e) water level.

3.2 Selection of Extreme Offshore-directed Sediment Transport Events

As mentioned earlier, cross-shore beach profile surveys were conducted continuously (approximately once per day) along the pier. In this study, data from January 1987 to December 2003 were used, resulting in approximately 6,209 profiles over the 16 years. This section discusses the down-selection of data, resulting in extreme offshore dominant sediment transport events. In the down-selection process, we focus on identifying cross-shore dominant sediment transport events for which the volume of sediment is conserved within the profile.

3.2.1 Selection of Cross-shore Dominant Sediment Transport Events

Figure 3 presents the averaged beach profile and the standard deviation for all 6,209 profiles. Two peaks are visible in the mean profile, one at $x = -35$ m at the berm area landward of the mean water line and another at $x = 185$ m at the outer bar. Occasionally, an inner bar forms in the inner surf zone (0 m < x < 180 m), but this inner bar feature was ephemeral and not retained in the mean profile. It is noted that periodic features are visible in the region 200 m < x < 385 m due to the pilings supporting the pier. To select the onshore- and offshore-directed sediment transport cases, the cross-shore distance of the beach profile was separated into three zones based on the two peaks in the averaged beach profile: the foreshore zone (-115 m < x < -20 m), the nearshore zone (-15 m < x < 180 m) and the bar offshore zone (185 m < x < 385 m) and are denoted with subscripts “F” (foreshore), “N” (nearshore) and “B” (bar offshore).

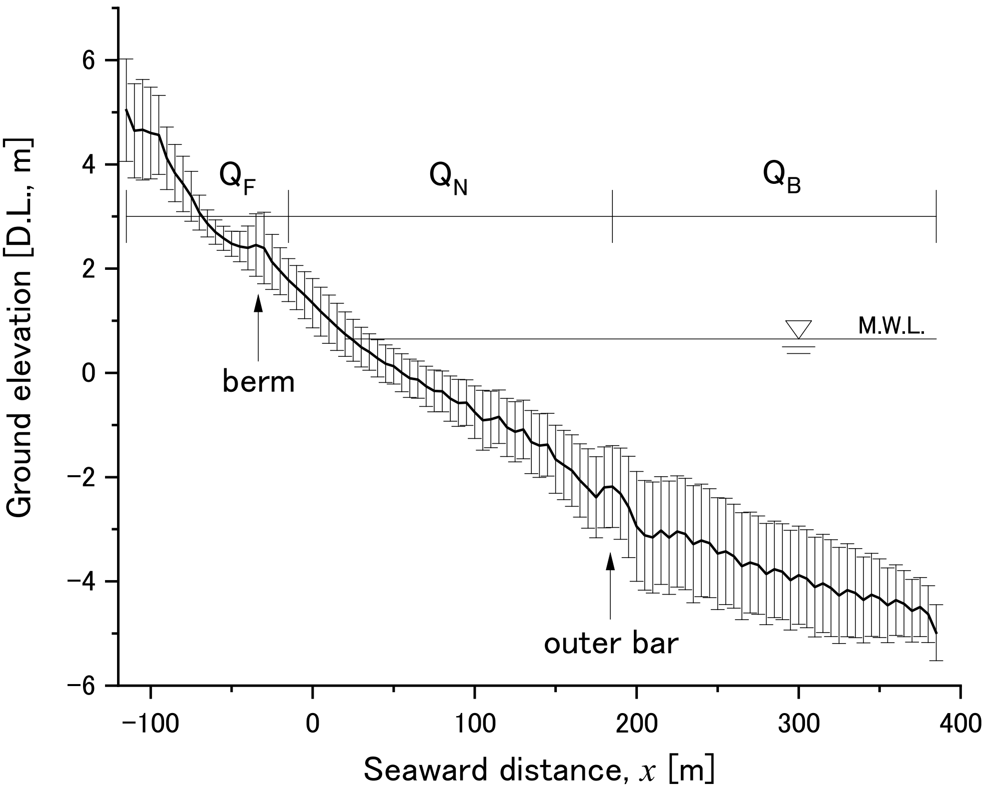

Figure 3. Averaged beach profile and its standard deviation using, the data from Jan. 1987 to Dec. 2003.

The volume difference, Q [m^3/m], over three days was calculated for each zone, that is $Q = Q(t) – Q(t\text{-}3)$, where t is the time in days, and denoted as Q_F (foreshore), Q_N (nearshore), and Q_B (bar offshore). The volume difference for the total profile (−115 m $< x <$ 385 m) was also calculated, Q_T. Values for which $Q < 0$ indicate offshore-directed transport.

The following procedure was used to down-select the data:

1. Focusing on nearshore sediment transport, we discriminated between onshore and offshore events. This yielded 3318 onshore events ($\sum Q_N > 0$) and 2888 offshore-directed events ($\sum Q_N < 0$) in the nearshore.
2. Considering a closed system where the sediment mass is conserved in the cross-shore, we chose events for which the total transport normalized by the total magnitude of transport was less than 10 % ($\sum Q_T / \sum |Q_T| < 0.1$). This reduced the number of nearshore onshore events from 3318 to 470 and the number of offshore-directed events from 2888 to 605.
3. We considered cases for which the longshore current at the nearshore zone, x = 145 m, was less than 0.25 m/s because this is a reasonable estimate of the critical value for the initiation of sediment transport, further reducing the cases to 285 onshore and 346 offshore-directed events.
4. We considered events for which there was a fairly large signal in the onshore or offshore-directed event defined as $\sum Q_N > 2$ [m^3/m], causing a reduction to 69 onshore and 101 offshore-directed events.
5. We considered events that occurred only on weekdays. Moreover, we also eliminated events lacking complete hydrodynamic data due to instrument failure, maintenance or replacement. This reduced the cases to 9 onshore and 17 offshore-directed events.

In summary, our down-selection process reduced the cases to be considered from 6,206 to 26 events.

3.2.2 Selection of Extreme Offshore-directed Sediment Transport Events

Despite the above reduction, it was necessary to examine each profile to select a reasonable final number of events for comparison with XBeach. Figure 4 illustrates the correlation between the volume difference in the nearshore zone Q_N and that in the bar offshore zone Q_B for the selected offshore/onshore dominant events. The cross symbol indicates the averaged values, and the error bars indicate the standard deviation, σ. All the events have negative correlations for the offshore dominant events, and sediment in the nearshore zone moves to the bar offshore zone. For the offshore dominant events, three events were larger than the value of 2σ. Here, the focus is on three extreme events that are numbered from ID1 to ID3.

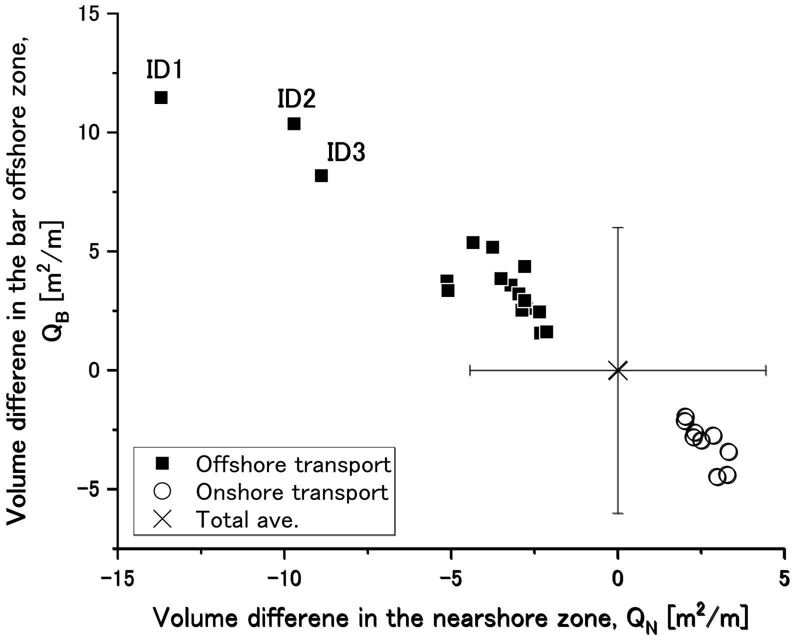

Figure 4: Correlation between volume difference in the nearshore zone, Q_N, and that in the bar offshore zone, Q_B.

Table 2 summarize the volume differences at each zone, longshore current at the cross-shore location of x = 145 m for the selected three extreme offshore-directed sediment transport events, and the last row lists the average, standard deviation, maximum and minimum values calculated using the dataset from 1987 to 2003 for the reference. We note here that two extreme offshore-directed sediment transport events ($\sum Q_N$ = -11.41 m^3/m and -10.72 m^3/m) were neglected because the longshore current at x = 145 m was large ($\langle | v_{145m} | \rangle$ = 0.430 m/s and 0.277 m/s) for these two events.

Table 2. Selected three extreme offshore-directed sediment transport events of volume difference at each zone.

ID	Date		$\sum Q_F$ [m^3/m]	$\sum Q_N$ [m^3/m]	$\sum Q_B$ [m^3/m]	$\sum Q_T$ [m^3/m]	$\sum \lvert Q_T \rvert$ [m^3/m]	$\frac{\sum Q_T}{\sum \lvert Q_T \rvert}$	$\langle \lvert v_{145m} \rvert \rangle$ [m/s]
1	1988/ 9/19-22		0.40	-13.69	11.46	-1.83	36.1	-0.051	0.220
2	1990/10/15-18		0.10	-9.70	10.36	0.76	24.1	0.032	0.151
3	1993/10/4-7		0.10	-8.88	8.17	-0.61	24.8	-0.025	0.218
Full data	1987/ 1/1– 2003/ 12/31	Ave	0.012	0.0056	–0.006	0.012	15.3	0.050	0.246
		std	0.346	4.44	6.01	8.30	8.21	0.415	0.138
		Max	1.89	23.3	36.89	47.6	84.8	0.960	0.963
		Min	–4.84	–29.3	–52.0	–59.5	2.71	–0.980	0.004

Figure 5 presents the wave conditions for the selected offshore/onshore dominant events. The cross symbol indicates the averaged values, and the error bars depict the standard deviations. The extreme offshore dominant events are marked as ID1, 2, and 3, and no significant trend can be seen for the extreme events, meaning that the wave height and periods that produced these events were within the range of the other events.

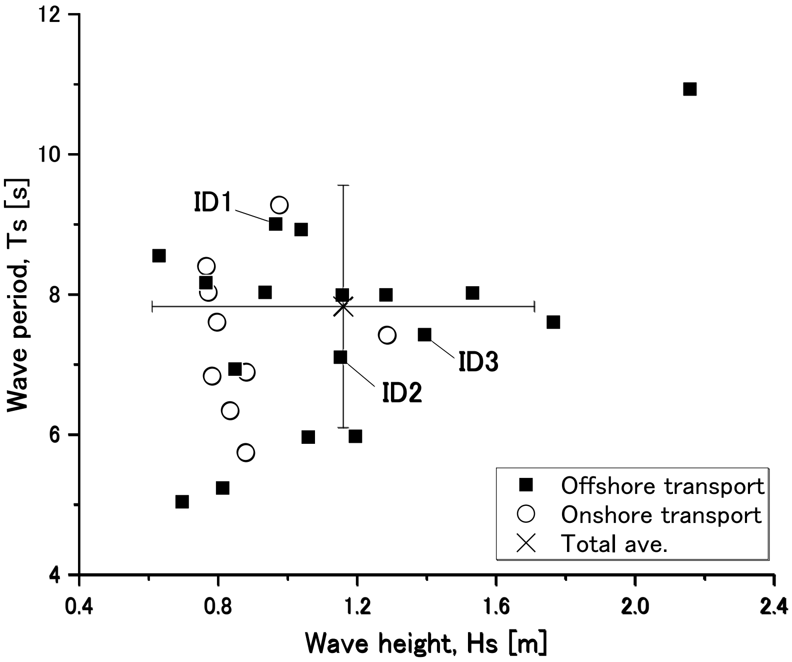

Figure 5: Correlation between significant wave height and wave period.

Table 3 lists the wave conditions for each extreme offshore-directed event. Figure 2 displayed a representative sample of the data corresponding to ID 2. Although it can be seen that ID 1 and 3 have similar wave periods that are somewhat lower than the mean period, the mean significant wave heights for each of the three events are typical of the wave heights for this area.

Table 3. Wave conditions of selected three extreme offshore-directed sediment transport events.

ID	Date	$\langle H_s \rangle$ [m]		$\langle T_s \rangle$ [s]		Wave direction at x = 380 m, $\langle \theta \rangle$ [degree]
		Ave.	std	Ave.	std	
1	1988/ 9/19-22	0.97	0.24	9.00	1.06	8.1
2	1990/10/15-18	1.15	0.17	7.10	1.19	17.5
3	1993/10/4-7	1.40	0.22	7.42	1.30	7.3
Full data	1987.1.1– 2003.12.31	1.16	0.55	7.83	1.73	15.3

Figure 6 shows the beach profile change and the volume change of the three selected extreme offshore-directed sediment transport events: (a) ID 1, (b) ID 2, and (c) ID 3. The top panel in each subplot exhibits the pre- and post-event cross-shore profiles and mean water level. The bottom panel displays the resulting sediment transport, Q, over the three days. The light dashed vertical lines in the figure indicate the three zones (foreshore, nearshore, and bar offshore). All the events are somewhat similar in that sediment transported offshore-ward from a relatively wide section of the nearshore zone (80 m < x < 190 m) and deposited in a relatively narrow portion of the offshore bar area (190 m < x < 240 m). Moreover, some sediment deposition occurred at the onshore end of the eroded area in the nearshore zone.

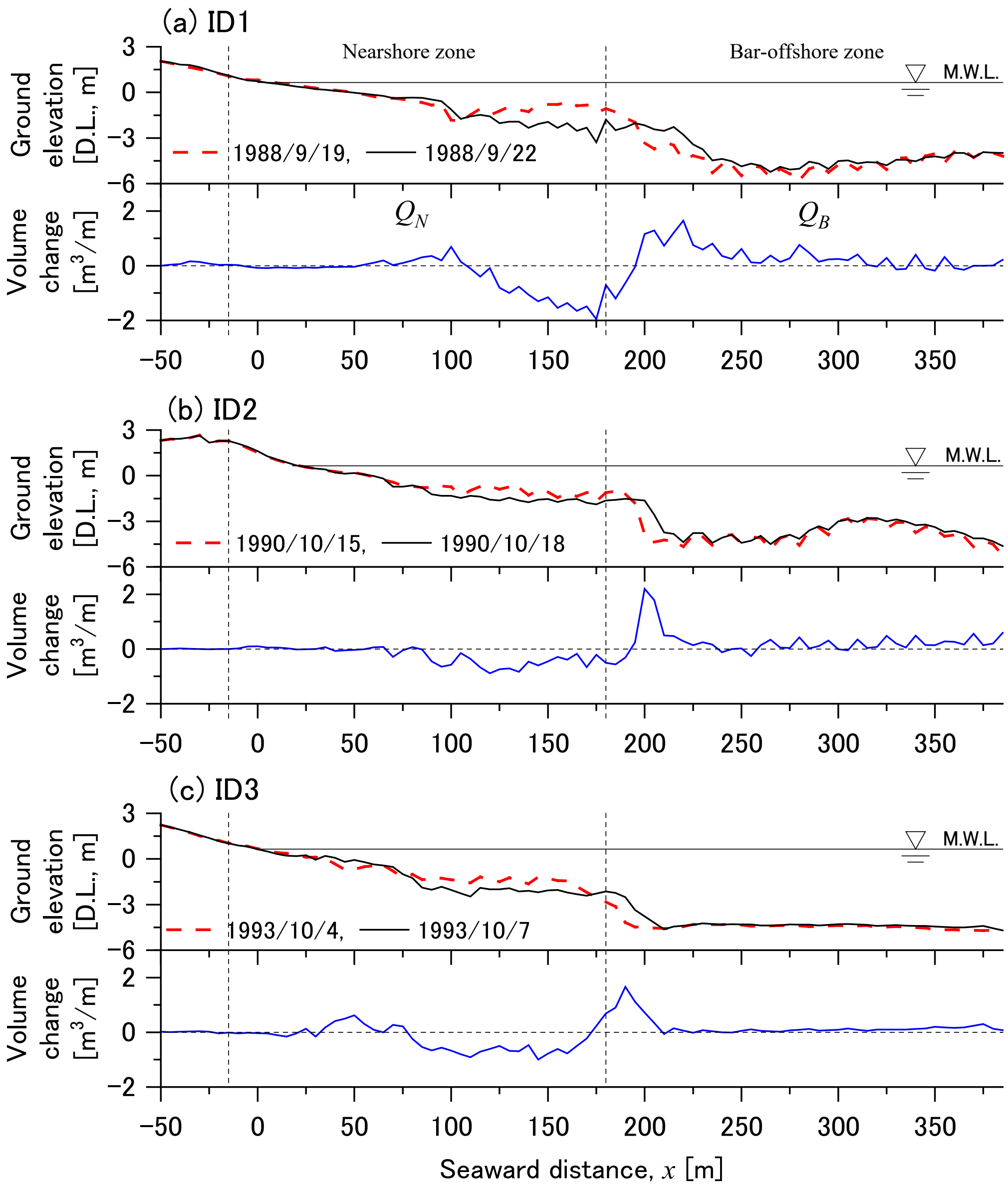

Figure 6: Beach profile change and volume change of extreme offshore-directed sediment transport events. (a) ID1, 1988/9/19–22, (b) ID2, 1990/10/15–18, and (c) ID3, 1993/10/4–7.

3.3 XBeach Setup and Error Metrics

The XBeach domain was 500 m in the cross-shore direction with a grid resolution of 5 m for the longshore direction, that is, the 1-D model. The location of the offshore boundary is the same as the pier end of the HORS. The median diameter d_{50} is set as the same median diameter at the Hasaki coast, 0.18 mm. The wave height and period inputs at the offshore boundary were created using a JONSWAP spectrum with default parameters, and the H_{mo} and T_p observed waves at the end of the pier. As explained earlier, the wave angle at the pier was estimated using Snell's law from the offshore ultrasonic sensor. Tidal variation was also included at the offshore boundary. Since cross-shore dominant sediment transport events were selected, the effect of longshore current was neglected in this analysis. Table 4 lists the summary of the main parameter values used in this study. The other XBeach hydrodynamic and morphodynamic parameters were set as default values.

Table 4. XBeach parameters for the selected events.

Parameter description	Default	Used in this analysis
Wave breaking parameter	Roelvink extended	Daly et al.
Sed. transport formula	vanthiel_vanrijn	soulsby_vanrijn
Morphological Accel. param.: f_{mor}	1	5
Wave nonlinearity param.: f_{ua}	0.1	0 – 0.55
Bed friction (Chezy): C	55	30

The performance of XBeach on the prediction of wave height and beach profile change can be evaluated on the basis of the relative mean absolute error (RMAE) and Brier Skill Score (BSS), respectively. The formulae are as follows (e.g., van Rijn et al., 2003):

$$\mathrm{RMAE} = \left\langle \left| H_c - H_m \right| - \Delta H_m \right\rangle \Big/ \left\langle H_m \right\rangle \tag{8}$$

$$\mathrm{BSS} = 1 - \left[\left\langle (| z_{b,c} - z_{b,m} | - \Delta z_{b,m})^2 \right\rangle \Big/ \left\langle (z_{b,0} - z_{b,m})^2 \right\rangle \right] \tag{9}$$

where indexes m and c are measured and computed. H is the wave height, z_b is the bed level, ΔH_m and $\Delta z_{b,m}$ are the errors of the measured wave height and bed level, $z_{b,0}$ is the initial bed level, and $\langle \ldots \rangle$ is the averaging procedure over the time series. Table 5 lists the qualifications of the model performance (excellent, good, etc.) based on the RMAE and BSS ranges. It is noted that the statistic parameters of wave height and bed level are corrected for the measurement errors being ΔH_m = 0.1 m and $\Delta z_{b,m}$ = 0.1 m in field conditions (van Rijn et al., 2000). In this analysis, ΔH_m = 0.05 m and $\Delta z_{b,m}$ = 0.05 m are used.

Table 5. Qualification of error ranges of process parameters (van Rijn et al., 2003).

Qualification	Wave height RMAE	Morphology BSS
Excellent	< 0.05	1.0 – 0.8
Good	0.05 – 0.1	0.8 – 0.6
Fair	0.1 – 0.2	0.6 – 0.3
Poor	0.2 – 0.3	0.3 – 0

Bad	> 0.3	< 0

5. Analysis and discussion of extreme offshore-directed sediment transport repeatability

5.1 Effect of wave breaking parameter on wave height

In this section, the effect of the wave breaking formulations on the wave height variation inside the surf zone and the effect of wave nonlinearity on beach profile change are discussed using the event, ID 2 (1990/10/15–18). Recalling Figure 2, the observations show relatively high wave conditions before and during the event (Fig. 2a). The wave direction during the event was coming from northward (2c) yet the longshore current remained relatively small and less than 0.25 m/s during the event (2d). The statistical values of the observed data at the pier end during the event are listed in Table 3, and the ranges of the values are 0.86 m < H_s < 1.67 m and 5.3 s < T_s < 9.9 s.

Figure 7 shows the observed and calculated wave height time series at x = 380 m, 145 m, and 40 m using both wave breaking formulations (Roelvink extended and Daly et al.). The solid line indicates the observed data, blue, green, and red lines indicate the Roelvink extended with the default γ = 0.55, calibrated γ = 0.20, and Daly et al. formula with calibrated γ = 0.80 and γ_2 = 0.10, respectively.

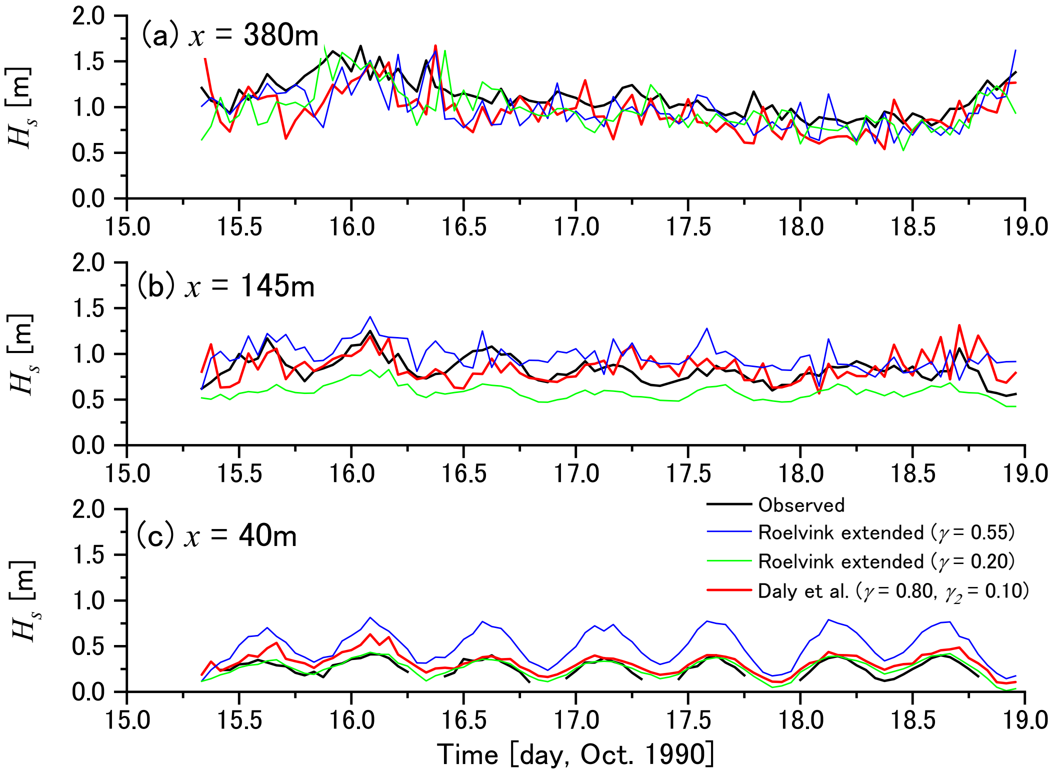

Figure 7: Observed and simulated wave height using extended Roelvink and Daly et al. wave breaking formulations. (a) x = 380 m, (b) x = 145 m, and (c) x = 40 m.

The Roelvink extended formulation with default γ (= 0.55) indicates that the wave height at x = 380 m and 145 m show reasonable agreement with RMAE values of 0.11 and 0.16, respectively. However, at x = 40 m, the wave height is overestimated with a bad agreement (RMAE = 0.94). This indicates that the wave breaking model with default γ does not adequately reduce the wave energy due to wave breaking. With tuning using γ = 0.20, it was possible to obtain excellent results at x = 40 m (RMAE = 0.04) and reasonable agreement at x = 380 (RMAE = 0.11). However, the wave heights were underestimated with poor agreement at x = 145 m (RMAE = 0.24). In summary, it was not possible to tune the Roelvink extended formulation with a single value to provide adequate agreement at all three locations in the surf zone. In contrast, the formulation of Daly et al. (red lines) shows reasonable results at all three locations: x = 380 m (RMAE = 0.11), 145 m (RMAE = 0.10) and 40 m (RMAE = 0.16). Table 6 summarizes the wave height comparisons.

Therefore, the wave-breaking formulation of Daly et al. with tuned the breaker indexes γ and γ_2 for each event was used for the sediment transport comparison in the next section.

Table 6: Wave breaking formulations and its parameter values and RMAE of each formulation.

Wave breaking model	RMAE of H_s [m]		
	x = 380 m	x = 145 m	x = 40 m
Roelvink extended, γ = 0.55	0.11 Fair	0.16 Fair	0.94 Bad
Roelvink extended, γ = 0.20	0.12 Fair	0.24 Poor	0.04 Excellent
Daly et al., γ = 0.80, γ_2 = 0.10	0.14 Fair	0.10 Good	0.16 Fair

5.2 XBeach cross-shore sediment transport prediction

As mentioned previously, the effect of wave nonlinearity on sediment transport was modeled in XBeach using wave skewness and asymmetry parameters. The parameter f_{ua}

can change both parameters simultaneously and is discussed in detail in this section. Similar to the wave comparison, the BSS is also used for model-data comparison of the morphological change. For all the events, almost no profile change occurred in the foreshore zone (-115 m < x < -20 m). Therefore, the BSS is calculated for the nearshore zone (BSS_N: -15 m < x < 180 m), bar offshore zone (BSS_B: 185 m < x < 385 m), and combined nearshore and bar offshore zones (BSS_{NB}: -15 m < x < 385 m). The wave nonlinearity parameter, f_{ua}, is calibrated to fit the beach profile change with the observed data for each event. Since the wave propagation was adjusted as discussed in section 5.1, the model's predictive skill is related to the morphodynamic parameters, e.g., f_{ua}.

Figure 8 displays the correlation between the f_{ua} and BSS for different zones. In the nearshore zone, panel (a), all the events exhibit nearly the same trend, wherein f_{ua} = 0.0 is the best result; however, the qualification is fair. The BSS_N values gradually decrease when the f_{ua} increase and become a bad rank. Conversely, in the bar-offshore zone, panel (b), although BSS_B for ID1 is a fair rank at f_{ua} = 0.0, and almost constant at 0.23, IDs 2 and 3 are excellent ranks at low f_{ua} (<0.05). For ID2 and 3, BSS_B gradually decreased when the f_{ua} increased. Panel (c) shows the BSS of the area includes both nearshore and bar-offshore zones (BSS_{NB}; -15 m < x < 385 m). All the values of BSS_{NBS} decrease when the number of f_{ua} increases. Overall, for the extreme offshore-directed sediment transport events, f_{ua} = 0.0 displayed the best fit. Table 7 lists the best BSS using f_{ua} = 0.0 for each zone.

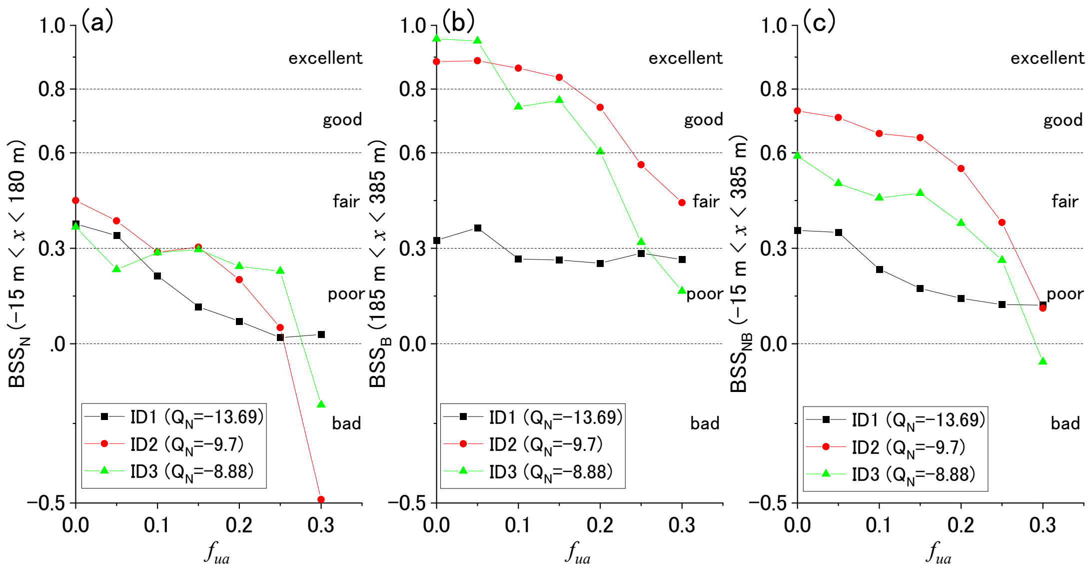

Figure 8: Sensitivity of nonlinearity parameter, f_{ua}, on beach profile prediction. (a) nearshore zone, BSS_N, (b) bar offshore zone, BSS_B, (c) nearshore and bar-offshore zones, BSS_{NB}.

Table 7. BSS of each cross-shore zone during extreme offshore-directed sediment transport events.

ID	Nearshore zone, BSS_N	Bar-offshore zone, BSS_B	Nearshore and bar-offshore zones, BSS_{NB}
1	0.377	0.325	0.356
2	0.450	0.886	0.731
3	0.367	0.957	0.590

Here, using the f_{ua} = 0.0, the volume change of the observed (dashed line) and calculated (solid line) results for ID1, 2, and 3 are depicted in Figures 9(a), (b), and (c), respectively. In the nearshore zone, although all the events are underestimated, the trends of the spatial distributions are similar to that of the observed results. The beach profile near the shoreline area, observed results show small deposition or even; however, calculated results show erosion for all the events. In the bar-offshore zone, except for ID1, the peak of the volume change showed good agreement. For ID1, the peak of the onshore end is the same as the observed results, XBeach could not simulate the sediment movement at the offshore side of x = 215 m.

In this analysis, the JONSWAP spectrum was used for the incident wave. Therefore, the role of infragravity waves was not taken into account in these simulations. It could be considered that this is one of the reasons that the best fit f_{ua} = 0 and the mismatch between the observed and simulated beach profile change.

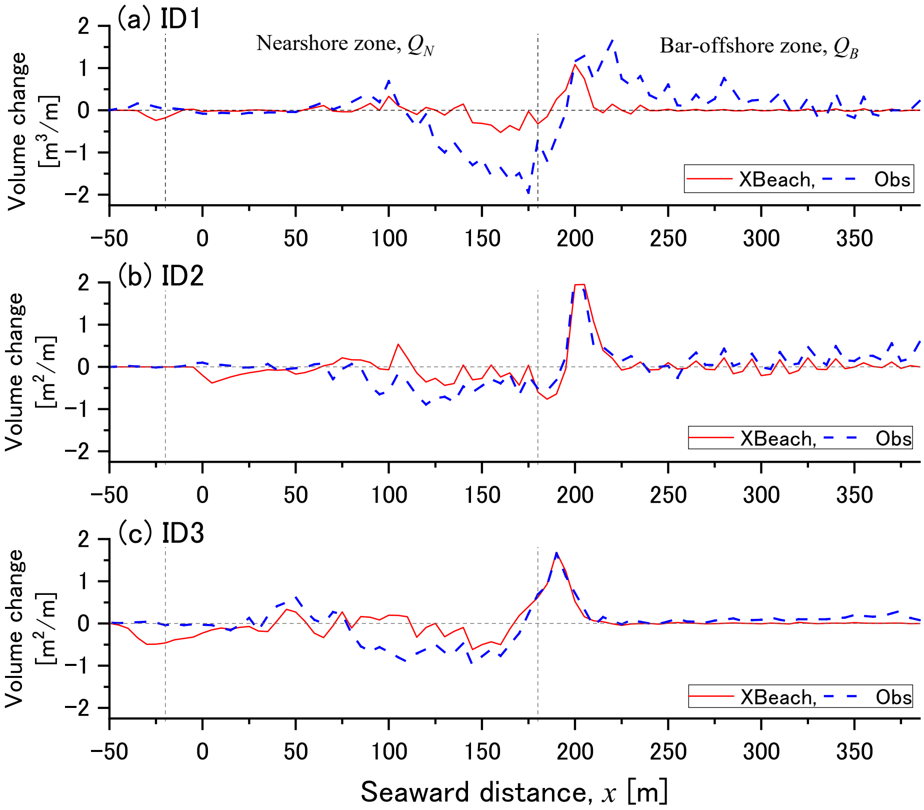

Figure 9: Volume change of observed and calculated results. (a) ID 1, (b) ID2, and (c) ID 3.

Figure 10 of panels (a) and (b) illustrate the correlation between the volume change and f_{ua}, and volume change and BSS, respectively. In this figure, the selected 17 offshore dominant events are plotted, and three extreme events that is ID1-3, are marked with open circles. The red circles and solid squares are the data of the nearshore zone and bar-offshore zone, respectively. All the events, wave breaking parameters of breaker indexes, and f_{ua} were tuned as the profile BSS indicated the highest value.

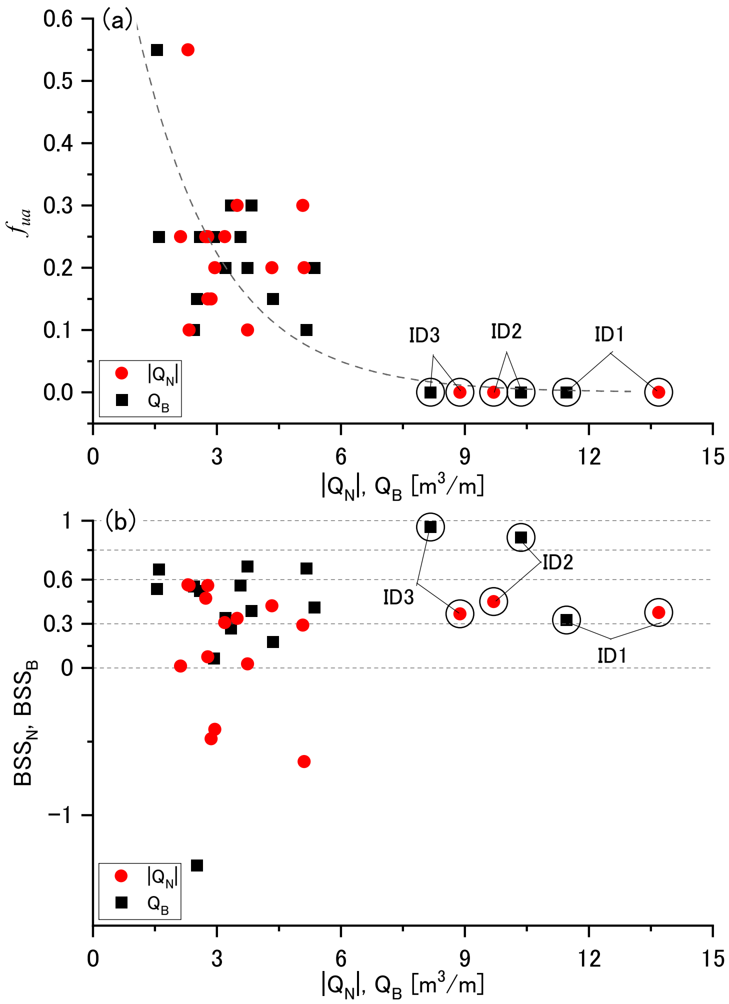

Figure 10: (a) correlation between volume change and f_{ua}, (b) correlation between volume change and BSS. The selected 17 offshore dominant events are plotted and three extreme events that are ID1-3, are marked with open circles. The red circles and solid squares are the data of the nearshore zone and bar-offshore zone, respectively.

The correlation between Q_N and f_{ua} displays a negative correlation (panel (a) of red circles). Although bad qualifications include a range of $2 < |Q_N| < 6$ (panel (b) of red circles), the relation can be expressed as: $f_{ua} = e^{0.5Q_N}$ $(R^2 = 0.26)$. Panels (a) and (b) of solid squares present the comparison of Q_B. The parameter f_{ua} has a negative correlation and can be estimated using Q_B as $f_{ua} = e^{-0.5Q_B}$ $(R^2 = 0.43)$. The BSS value is slightly better than that of the Q_N (panel (b) of solid squares). Although the correction coefficients with volume changes and BSS_N, BSS_B are not high, we could see the relation curve between the two. Thus, if we could expect the volume change at the beach based on the past observed data, shoreline, etc., or find another parameter that could estimate volume change, we can decide f_{ua} and may calculate the appropriate beach profile change.

Elsayed et al. (2017) proposed the f_{ua} estimate equation using average beach slope steepness, $S_s = \tan\beta$, and showed a good correlation, $R^2 = 0.77$. Following their method, we also analyzed the correlation between the two, the averaged beach slope of nearshore to bar-offshore zone, i.e., x = -15 m to 385 m, and f_{ua}. As a result, f_{ua} could show the correction with the power function of $f_{ua} = 1.34 \times 10^6 S_s^{3.83}$ $(R^2 = 0.29)$. Compared to the Elsayed et al. cases, since we are using filed data, the beach profile is much smaller (Elsayed et al.: $0.06 < S_s < 0.158$; present study: $0.013 < S_s < 0.019$), maybe this is one of the reasons that the correction coefficient was low.

Moreover, earlier attempts to relate f_{ua} to wave energy flux and sediment fall velocity (used Dean Number) were unsuccessful (R^2 = 0.03 and 0.02, respectively). This is not surprising given that the wave heights and periods for the extreme events were not out of the ordinary (Fig. 5). It could be said that short waves are not the main reason for offshore-directed sediment transport for the three selected events. This suggests that, perhaps, the antecedent profile conditions play a role or that the sediment transport occurs at a time scale faster than what is being used to characterize the hydrodynamic conditions.

6. Conclusions

The performance of the sediment transport model XBeach for predicting the profile changes during extreme offshore-directed sediment transport events was investigated using field observations at a dissipative beach in Japan. The data were carefully down-selected to focus on events for which the majority of the sediment was primarily cross-shore directed based on several criteria, resulting in data for 17 events. Moreover, from these 17 events, the top three events were used to investigate the sensitivity of the nonlinearity parameter, f_{ua}, on beach profile prediction. In addition, by using all 17 selected events, the correlation between f_{ua} and volume change is discussed. The following conclusions can be drawn from this study.

For the extreme offshore-directed sediment transport events, $f_{ua} = 0.0$ is the best fit for predicting the beach profile change. The trend of beach erosion and accretion could be estimated well for all the events; however, in the nearshore zone, erosion tends to be underestimated and the BSS displays lower values. In the bar-offshore zone, sediments are transported from the nearshore zone, and peak sediment deposition occurs. In the simulation, these peak depositions were well estimated. Considering the correlation between volume change and the f_{ua} of the selected 17 offshore-directed sediment transport events, although the model could not accurately predict some events, the f_{ua} value may be estimated using the volume change.

In the future, other physical parameters such as the *P*-parameter or *JA*-predictor can be investigated to determine if they can provide suitable guidance on setting f_{ua} for offshore-directed sediment transport. The time-varying nature of these parameters should be explored. Moreover, the value of f_{ua} may change, depends on the beach forms. In this analysis, we used the data observed at the dissipative beach. Thus, we also need to investigate the performance of f_{ua} using data of reflective or intermediate beaches.

Acknowledgements

We express our thanks to reviewers for their valuable comments and discussion. We could improve by following the reviewer's suggestions. The authors also would like to thank the Coastal and Estuarine Sediment Dynamics Group, and Marine Information Group of Port and Airport Research Institute and Kashima Port and Airport Construction Office, for allowing the use of beach profile and wave data at the Hazaki Oceanographical Research Station and wave data from the Port of Kashima. This research was funded by JSPS Grants-in-Aid No. 26709034 and No. 15KK0202. The second author was supported by the National Science Foundation through OCE-1756449.

References

Armaroli, C., Grottoli, E., Harley, M. D., & Ciavola, P. (2013). Beach morphodynamics and types of foredune erosion generated by storms along the Emilia-Romagna coastline, Italy. *Geomorphology*, 199, 22-35. doi.org/10.1016/j.geomorph.2013.04.034

Bailard, J. A. (1981). An energetics total load sediment transport model for a plane sloping beach. *Journal of Geophysical Research: Oceans*, 86(C11), 10938-10954. doi.org/10.1029/JC086iC11p10938

Baldock, T. E., Alsina, J. A., Caceres, I., Vicinanza, D., Contestabile, P., Power, H., & Sanchez-Arcilla, A. (2011). Large-scale experiments on beach profile evolution and surf and swash zone sediment transport induced by long waves, wave groups and random waves. *Coastal Engineering*, 58(2), 214-227. doi.org/10.1016/j.coastaleng.2010.10.006

Berard, N. A., Mulligan, R. P., da Silva, A. M. F., & Dibajnia, M. (2017). Evaluation of XBeach performance for the erosion of a laboratory sand dune. *Coastal Engineering*, 125, 70-80. doi.org/10.1016/j.coastaleng.2017.04.002

Bolle, A., Mercelis, P., Roelvink, D., Haerens, P., & Trouw, K. (2010). Application and validation of XBeach for three different field sites. *Proceedings of 32nd International Conference on Coastal Engineering*, 1(32), 40. doi.org/10.9753/icce.v32.sediment.40

Bugajny, N., Furmańczyk, K., Dudzińska-Nowak, J., & Paplińska-Swerpel, B. (2013). Modelling morphological changes of beach and dune induced by storm on the Southern Baltic coast using XBeach (case study: Dziwnow Spit). Journal of Coastal Research, (65), 672-677. doi.org/10.2112/SI65-114.1

Callaghan, D. P., Ranasinghe, R., & Roelvink, D. (2013). Probabilistic estimation of storm erosion using analytical, semi-empirical, and process based storm erosion models. *Coastal Engineering*, 82, 64-75. doi.org/10.1016/j.coastaleng.2013.08.007

Deigaard, R., Fredsøe, J., & Hedegaard, I. B. (1986). Suspended sediment in the surf zone. *Journal of Waterway, Port, Coastal, and Ocean Engineering*, 112(1), 115-128. doi.org/10.1061/(ASCE)0733-950X(1986)112:1(115)

De Alegria-Arzaburu, A. R., Williams, J. J., & Masselink, G. (2010). Application of XBeach to model storm response on a macrotidal gravel barrier. *Proceedings of 32nd International Conference on Coastal Engineering*, 1(32), 39. doi.org/10.9753/icce.v32.sediment.39

De Vet, P. L. M., McCall, R. T., den Bieman, J. P., Stive, M. J., & van Ormondt, M. (2015). Modelling dune erosion, overwash and breaching at Fire Island (NY) during Hurricane Sandy. *Proceedings of Coastal Sediments*. doi:10.1142/9789814689977_0006

De Winter, R. C., Gongriep, F., & Ruessink, B. G. (2015). Observations and modeling of alongshore variability in dune erosion at Egmond aan Zee, the Netherlands. *Coastal Engineering*, 99, 167-175. doi.org/10.1016/j.coastaleng.2015.02.005

De Winter, R. C., & Ruessink, B. G. (2017). Sensitivity analysis of climate change impacts on dune erosion: case study for the Dutch Holland coast. *Climatic Change*, 141(4), 685-701. doi.org/10.1007/s11069-014-1417-8

Dissanayake, P., Brown, J., & Karunarathna, H. (2014). Modelling storm-induced beach/dune evolution: Sefton coast, Liverpool Bay, UK. *Marine Geology*, 357, 225-242. doi.org/10.1016/j.margeo.2014.07.013

Do, K., Shin, S., Cox, D., & Yoo, J. (2018). Numerical Simulation and Large-Scale Physical Modelling of Coastal Sand Dune Erosion. *Journal of Coastal Research*, SI, 85, 196-200. doi.org/10.2112/SI85-040.1

Elgar, S., Gallagher, E. L., & Guza, R. T. (2001). Nearshore sandbar migration. *Journal of Geophysical Research: Oceans*, 106(C6), 11623-11627. doi.org/10.1029/2000JC000389

Elsayed, S. M., & Oumeraci, H. (2017). Effect of beach slope and grain-stabilization on coastal sediment transport: An attempt to overcome the erosion overestimation by XBeach. *Coastal Engineering*, 121, 179-196. doi.org/10.1016/j.coastaleng.2016.12.009

Faraci, C., Scandura, P., & Foti, E. (2014). Bottom profile evolution of a perched nourished beach. *Journal of Waterway, Port, Coastal, and Ocean Engineering*, 140(5), 04014021. doi.org/10.1061/(ASCE)WW.1943-5460.0000253

Figlus, J., Kobayashi, N., Gralher, C., & Iranzo, V. (2011). Wave overtopping and overwash of dunes, *Journal of Waterway, Port, Coastal, and Ocean Engineering*, 137(1), 26-33. doi.org/10.1061/(ASCE)WW.1943-5460.0000060

Galappatti, G., & Vreugdenhil, C. B. (1985). A depth-integrated model for suspended sediment transport. *Journal of Hydraulic Research*, 23(4), 359-377. doi.org/10.1080/00221688509499345

Jamal, M. H., Simmonds, D. J., & Magar, V. (2014). Modelling gravel beach dynamics with XBeach. *Coastal Engineering*, 89, 20-29. doi.org/10.1016/j.coastaleng.2014.03.006

Jayaratne, M. P. R., Rahman, M. R., & Shibayama, T. (2014). A cross-shore beach profile evolution model. *Coastal Engineering Journal*, 56(4), 1450020. doi.org/10.1142/S057856341450020X

Kotah, K., & Yanagishima, S. (1988). Predictive model for daily changes of shoreline. *Proceedings of 21st International Conference on Coastal Engineering*, 1(21). doi.org/10.1061/9780872626874.094

Katoh, K., & Yanagishima, S. (1995). Changes of sand grain distribution in the surf zone. *Proceedings of Coastal Dynamics*, 639-650.

Kelly, D. M., & Dodd, N. (2010). Beach-face evolution in the swash zone. *Journal of Fluid Mechanics*, 661, 316-340. doi.org/10.1017/S0022112010002983

Kobayashi, N., & Farhadzadeh, A. (2008). Cross-shore numerical model CSHORE for waves, currents, sediment transport and beach profile evolution. *Research Rep. No. CACR-08-01*, Center for Applied Coastal Research, Univ. of Delaware, Newark, Del. https://hdl.handle.net/11681/7734

Kuriyama, Y. (2002). Medium-term bar behavior and associated sediment transport at Hasaki, Japan. *Journal of Geophysical Research: Oceans*, 107(C9), 15-1, doi.org/10.1029/2001JC000899

Kuriyama, Y., Ito, Y., & Yanagishima, S. (2008). Cross-shore variation of long-term average longshore current velocity in the nearshore zone. *Continental Shelf Research*, 28(3), 491-502. doi.org/10.1016/j.csr.2007.10.008

Kuriyama, Y. (2012). Process-based one-dimensional model for cyclic longshore bar evolution. *Coastal Engineering*, 62, 48-61. doi.org/10.1016/j.coastaleng.2011.12.001

Larson, M., & Kraus, N. C. (1989). SBEACH: numerical model for simulating storm-induced beach change. Report 1. *Empirical foundation and model development (No. CERC-TR-89-9)*. Coastal Engineering Research Center, Vicksburg, MS.

Larson, M., Kubota, S., & Erikson, L. (2004). Swash-zone sediment transport and foreshore evolution: field experiments and mathematical modeling. *Marine Geology*, 212(1-4), 61-79. doi.org/10.1016/j.margeo.2004.08.004

Lindemer, C. A., Plant, N. G., Puleo, J. A., Thompson, D. M., & Wamsley, T. V. (2010). Numerical simulation of a low-lying barrier island's morphological response to Hurricane Katrina. *Coastal Engineering*, 57(11-12), 985-995. doi.org/10.1016/j.coastaleng.2010.06.004

McCall, R. T., De Vries, J. V. T., Plant, N. G., Van Dongeren, A. R., Roelvink, J. A., Thompson, D. M., & Reniers, A. J. H. M. (2010). Two-dimensional time dependent hurricane overwash and erosion modeling at Santa Rosa Island. *Coastal Engineering*, 57(7), 668-683. doi.org/10.1016/j.coastaleng.2010.02.006

Nederhoff, C. M., Lodder, Q. J., Boers, M., Den Bieman, J. P., & Miller, J. K. (2015). Modeling the effects of hard structures on dune erosion and overwash: A case study of the impact of Hurricane Sandy on the New Jersey coast. In The Proceedings of the Coastal Sediments 2015. doi.org/10.1142/9789814689977_0219

Palmsten, M. L., & Splinter, K. D. (2016). Observations and simulations of wave runup during a laboratory dune erosion experiment. *Coastal Engineering*, 115, 58-66. doi.org/10.1016/j.coastaleng.2016.01.007

Pender, D., & Karunarathna, H. (2013). A statistical-process based approach for modelling beach profile variability. *Coastal Engineering*, 81, 19-29. oi.org/10.1016/j.coastaleng.2013.06.006

Puleo, J. A., Beach, R. A., Holman, R. A., & Allen, J. S. (2000). Swash zone sediment suspension and transport and the importance of bore-generated turbulence. *Journal of Geophysical Research: Oceans*, 105(C7), 17021-17044. doi.org/10.1016/j.coastaleng.2013.06.006

Rafati, Y., Hsu, T. J., Elgar, S., Raubenheimer, B., Quataert, E., & van Dongeren, A. (2021). Modeling the hydrodynamics and morphodynamics of sandbar migration events. Coastal Engineering, 166, 103885. doi.org/10.1016/j.coastaleng.2021.103885

Roelvink, D., Reniers, A., Van Dongeren, A. P., de Vries, J. V. T., McCall, R., & Lescinski, J. (2009). Modelling storm impacts on beaches, dunes and barrier islands. *Coastal Engineering*, 56(11-12), 1133-1152. doi.org/10.1016/j.coastaleng.2009.08.006

Roelvink, D., McCall, R., Mehvar, S., Nederhoff, K., & Dastgheib, A. (2018). Improving predictions of swash dynamics in XBeach: The role of groupiness and incident-band runup. *Coastal Engineering*, 134, 103-123. doi.org/10.1016/j.coastaleng.2017.07.004

Schambach, L., Grilli, A. R., Grilli, S. T., Hashemi, M. R., & King, J. W. (2018). Assessing the impact of extreme storms on barrier beaches along the Atlantic coastline: Application to the southern Rhode Island coast. *Coastal Engineering*, 133, 26-42. doi.org/10.1016/j.coastaleng.2017.12.004

Schweiger, C., Kaehler, C., Koldrack, N., & Schuettrumpf, H. (2020). Spatial and temporal evaluation of storm-induced erosion modelling based on a two-dimensional field case including an artificial unvegetated research dune. *Coastal Engineering*, 161, 103752. doi.org/10.1016/j.coastaleng.2020.103752

Splinter, K. D., & Palmsten, M. L. (2012). Modeling dune response to an East Coast Low. *Marine Geology*, 329, 46-57. doi.org/10.1016/j.margeo.2012.09.005

Splinter, K. D., Carley, J. T., Golshani, A., & Tomlinson, R. (2014). A relationship to describe the cumulative impact of storm clusters on beach erosion. *Coastal Engineering*, 83, 49-55. doi.org/10.1016/j.coastaleng.2013.10.001

Suzuki, T., Takeuchi, M., Tomoda, N., Yamaguchi, S., & Kuriyama, Y. (2007). Spatial distribution of cross-shore sediment transport rate for berm formation and erosion. *Proceedings of Coastal Sediments*, 7, 2037-2048. doi.org/10.1061/40926(239)160

Suzuki, T., Mori, N., & Cox, D. T. (2009). Statistical modeling of near-bed pressure gradients measured on a natural beach. *Coastal Engineering Journal*, 51(02), 101-121. doi.org/10.1142/S0578563409001965

Suzuki, T., Inami, Y., Yanagishima, S., Sakihama, S., & Cox, D. T. (2019). Sediment particle movements observed using tracers under accretive wave conditions in the nearshore zone. *Coastal Engineering Journal*. doi:10.1080/21664250.2019.1629863.

Van Rijn, L.C., Grasmeijer, B.T., Ruessink, B.G., 2000, Measurement errors of instruments for velocity, wave height, sand concentration and bed levels in field conditions. *COAST3D Report*, Delft Hydraulics, Delft, The Netherlands, 47p. http://resolver.tudelft.nl/uuid:eb375d04-87e6-49f3-b04a-4b2a1a2046f3

Van Rijn, L. C., Walstra, D. J. R., Grasmeijer, B., Sutherland, J., Pan, S., & Sierra, J. P. (2003). The predictability of cross-shore bed evolution of sandy beaches at the time scale of storms and seasons using process-based profile models. *Coastal Engineering*, 47(3), 295-327. doi.org/10.1016/S0378-3839(02)00120-5

Verheyen, B., Gruwez, V., Zimmermann, N., Bolle, A., & Wauters, P. (2014). Medium term time-dependent morphodynamic modelling of beach profile evolution in Ada, Ghana. In ICHE 2014. *Proceedings of the 11th International Conference on Hydroscience & Engineering*, 701-708. https://hdl.handle.net/20.500.11970/99493

Vousdoukas, M. I., Almeida, L. P., & Ferreira, Ó. (2011). Modelling storm-induced beach morphological change in a meso-tidal, reflective beach using XBeach. *Journal of Coastal Research*, SI, 1916-1920. https://www.jstor.org/stable/26482510

Williams, J. J., de Alegría-Arzaburu, A. R., McCall, R. T., & Van Dongeren, A. P. (2012). Modelling gravel barrier profile response to combined waves and tides using

XBeach: Laboratory and field results. *Coastal Engineering*, 63, 62-80. doi.org/10.1016/j.coastaleng.2011.12.010

Williams, J. J., Esteves, L. S., & Rochford, L. A. (2015). Modelling storm responses on a high-energy coastline with XBeach. *Modeling Earth Systems and Environment*, 1(1-2), 3. doi 10.1007/s40808-015-0003-8

Yin, K., Xu, S., Huang, W., Li, R., & Xiao, H. (2019). Modeling beach profile changes by typhoon impacts at Xiamen coast. *Natural Hazards*, 95(3), 783-804. doi.org/10.1007/s11069-018-3520-8